

Soft Robotics: From Torque Feedback Controlled Lightweight Robots to Intrinsically Compliant Systems

A. Albu-Schäffer, O. Eiberger, M. Grebenstein, S. Haddadin, Ch. Ott, T. Wimböck, S. Wolf, and Gerd Hirzinger

Institute of Robotics and Mechatronics
German Aerospace Center (DLR)

I. INTRODUCTION

After decades of intensive research, it seems that we get closer to the time when robots will finally leave the cages of industrial robotic workcells and start working in the vicinity of and together with humans. This is not only believed by robotics researchers, but meanwhile also by leading automotive and IT companies, and of course by some clear-sighted industrial robot manufacturers. Several technologies required for this new kind of robots reached the necessary level of performance, e.g. computing power, communication technologies, sensors, and electronics integration. However, it is clear that these human friendly robots will look very different from today's industrial robots. Rich sensory information, light-weight design and soft robotics features are required in order to reach the expected performance and safety during interaction with unknown environments or with humans. In this paper we will present and compare two approaches for reaching the aforementioned soft robotics features. The first one is the meanwhile mature technology of torque controlled light-weight robots developed during the past decade at DLR (arms, hands, a humanoid upper body, a crawler). Several products resulted from this research and are currently being commercialized through cooperations with different industrial partners (DLR-KUKA Lightweight Robot, DLR-HIT-Schunk Hand, DLR-Brainlab-KUKA medical robot). The second technology, still a topic of worldwide ongoing research, is variable compliance actuation which implements the soft robotics features mainly in hardware.

We will start by reviewing the main design and control ideas of actively controlled compliant systems using as examples the DLR arms, hands, and the humanoid manipulator Justin. We are taking these robots as a performance reference, which we are currently trying to outperform with new variable stiffness actuators. This will lead us to the motivation of the variable stiffness actuator design. We will present the main design ideas and our first results with the new actuator prototypes. Some experimental examples providing first validation of the performance and safety gain of this design approach finally will be presented.

II. MECHATRONIC LIGHT-WEIGHT ROBOT DESIGN WITH JOINT TORQUE SENSING

In this section a mechatronic design approach for obtaining robots with the desired light-weight and performance prop-

erties is briefly described. Following aspects are of particular relevance:

- Light-weight structures. Light-weight metals or composite materials are used for the robot links.
- High energy motors. In contrast to industrial robots, not high velocity motors, but motors with high torque at moderate speed, low energy loss and fast dynamic response are of interest. For that purpose special motors, the DLR-Robodrive, have been designed.
- Gearing with high load/weight ratio. HarmonicDrive gears are used.
- Integration of electronics into the joint structure, leading to a modular design. This allows the design of robots of increasing kinematic complexity based on integrated joints as in the case of the DLR humanoid Justin. Moreover, one obtains a self-contained system, well suited for autonomous, mobile applications.
- Full state measurement in the joints. As will be outlined in Sec. III, our robots use torque sensing in addition to position sensing, in order to implement compliant behavior and a smooth, vibration-free motion. The full state measurement in all joints is performed at a 3kHz cycle, using strain gauge-based torque-sensing, motor position sensing based on magneto-resistive encoders, and link-side position sensing based on potentiometers (used only as an additional sensors for safety considerations).
- Sensor redundancy for safety (e.g. for position, forces, torques).

These basic design ideas are used for the joints of arms, hands, and the torso of the upper body system Justin (Fig. I). Moreover, due to the fact that the joints are self-contained, it is straight-forward to combine these modules to obtain different kinematic configurations. For example, the fingers have been used to build up a crawler prototype. Fig. 2 shows the exploded view of one Lightweight Robot III (DLR-LWRIII) joint.

III. COMPLIANCE CONTROL FOR LIGHT-WEIGHT ARMS

In the next two sections, the framework used to implement active compliance control based on joint torque sensing is summarized. The light-weight design is obtained by using relatively high gear reduction ratios (typically 1:100 or 1:160), leading to joints which are hardly backdrivable and

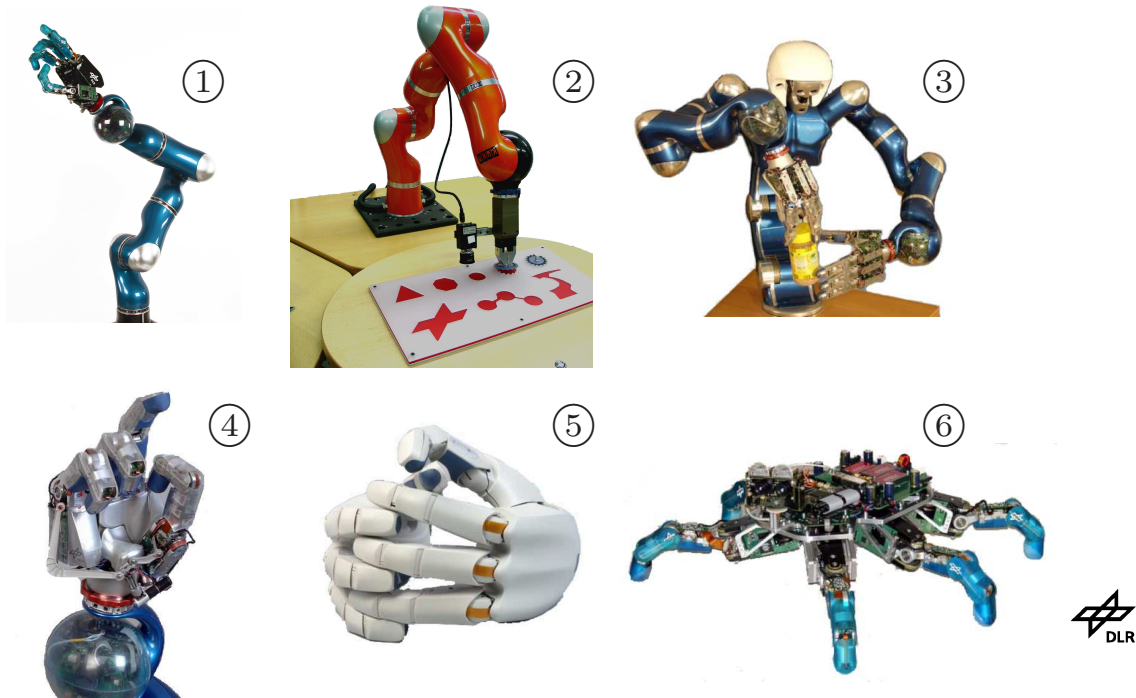


Fig. 1. Overview of the DLR Robots: ①: The DLR-LWRIII equipped with the DLR-HandII. ②: The DLR-KUKA-LWRIII which is based on the DLR-LWRIII. ③: The DLR Humanoid Manipulator “Justin”. ④: The DLR-HandII-b, a redesign of the DLR-HandII. ⑤: The DLR-HIT Hand, a commercialized version of the DLR-HandII. ⑥: The DLR-Crawler, a walking robot based on the fingers of the DLR-HandII.

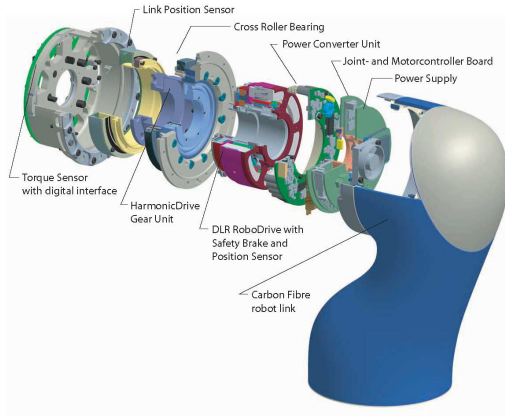


Fig. 2. The mechatronic joint design of the DLR-LWRIII including actuation, electronics, and sensing.

have already moderate intrinsic compliance. Therefore we model the robot as a flexible joint system. Thus, measuring the torque after the gears is essential for implementing high performance soft robotics features. When implementing compliant control laws, the torque signal is used for reducing both, the effects of joint friction as well as to damp vibrations related to the joint compliance. Motor position feedback is used to impose the desired compliant behavior. The control

framework is constructed from a passivity control perspective, by giving a simple and intuitive physical interpretation in terms of energy shaping to the feedback of the different state vector components.

- A physical interpretation of the joint torque feedback loop is given as the shaping of the motor inertia.
- The feedback of the motor position can be regarded as shaping of the potential energy.

A. Joint Torque Control: Shaping the Actuator Kinetic Energy

In order to simplify the analysis and to be able to generalize the joint level approach also to Cartesian coordinates, the idea of interpreting the joint torque feedback as the shaping of the motor inertia plays a central role [1], [2]. It enables to directly use the torque feedback within the passivity framework and conceptually divides the controller design into two steps. One is related to the torque feedback and the other to the position feedback, see Fig. 3. As sketched in the figure and presented in detail in [1], [2], the effect of the torque control loop is the reduction of the apparent motor inertia to a value B_θ , lower than the real value¹ B .

¹While friction is not depicted in Fig. 3, note that the frictional effect will be reduced by the same factor $B_\theta^{-1} B$.

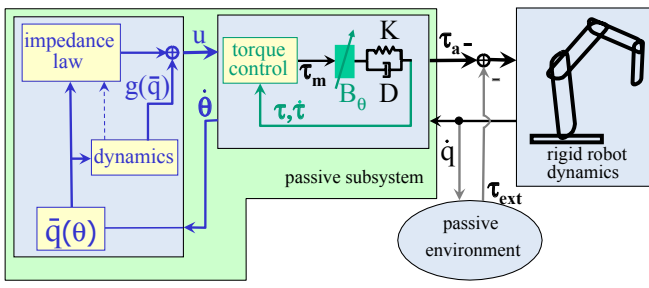


Fig. 3. Representation of the compliance controlled robot as a connection of passive blocks. θ is the motor position and q the link position. B , K and D are the motor inertia, joint stiffness, and damping matrices, respectively. τ is the elastic joint torque, τ_a the total (elastic and damping) joint torque, τ_{ext} the external torque, and g the gravity torque.

B. Motor Position Based Feedback: Shaping the Potential Energy

Using motor position θ for control and not the link position q is essential for the passivity properties of the controller. However, the desired position and stiffness are usually formulated in terms of the link position. For the impedance controllers of the DLR light-weight robots, the position feedback has the form

$$u = -\frac{\partial V_P(\bar{q}(\theta))}{\partial \theta} - D_\theta \dot{\theta} + g(\bar{q}(\theta)) \quad (1)$$

with u being the input to the torque controller, V_P a positive definite potential function, and D_θ a positive definite damping matrix chosen for a well damped transient behavior [3]. This is the classical structure of a compliance controller for rigid robots, except for the fact that, instead of the link position q , a position signal $\bar{q}(\theta)$ is used, which is *statically equivalent* to q , i.e. $\bar{q}(\theta) = q$ if $\dot{q} = \dot{\theta} = 0$ and can be computed numerically² [1], [2].

Since now the position feedback is again only a function of θ , the passivity of the controlled robot is given with respect to the input-output pair $(\tau_{\text{ext}}, \dot{q})$, see Fig. 3.

In order to obtain a joint level impedance controller, one can simply use $V_P(\bar{q}) = \frac{1}{2}(\mathbf{q}_d - \bar{\mathbf{q}})^T K_J(\mathbf{q}_d - \bar{\mathbf{q}})$, while for Cartesian impedance control V_P is defined as function of the Cartesian coordinates $\mathbf{x}(\bar{q})$ as detailed in section Sec. IV. The external torque τ_{ext} is then replaced by the external force³ \mathbf{F}_{ext} . A Lyapunov function for the system is obtained by summing the kinetic and the gravity-potential energy of the rigid part of the robot dynamics with the kinetic energy of the scaled motor inertia and the potential energy of the controller [1], [2].

IV. IMPEDANCE CONTROL FOR COMPLEX KINEMATIC CHAINS

In this section we show how to apply the impedance control concept from the previous section to kinematically

²In practice we often use indeed the trivial approximation $\bar{q}(\theta) = \theta$ for applications in which high position accuracy is not required.

³The relation between the external tip force \mathbf{F}_{ext} and the external joint torque τ_{ext} is $\tau_{\text{ext}} = \mathbf{J}(\bar{q})^T \mathbf{F}_{\text{ext}}$.

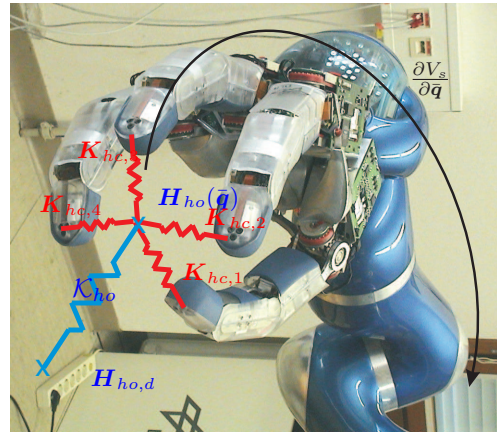


Fig. 4. DLR Hand II superimposed by the virtual springs defined by the potential functions in (2) and the virtual object.

more complex robot systems, like artificial hands and anthropomorphic two-handed manipulator systems. The design of appropriate potential functions $V_P(\bar{q})$ is the topic of this section. Furthermore, we will assume the potential function V_s of a virtual spatial spring, like e.g. the ones designed in [4], [5], [6], as a basic building block. This potential function $V_s(\mathbf{H}_1, \mathbf{H}_2, \mathcal{K})$ depends on two frames $\mathbf{H}_1 \in SE(3)$ and $\mathbf{H}_2 \in SE(3)$ between which the spring is acting, and also on some configuration-independent internal parameters \mathcal{K} , like the stiffness values or the rest length.

A. Artificial Hands

Similar to the DLR light-weight arm, the DLR hand II is equipped with joint torque sensors in addition to joint position measurements. Therefore, it is possible to apply the impedance control aspects as presented in the previous section to our anthropomorphic robot hand. The feedback of the torque sensors is used to increase the backdrivability, respectively the sensitivity, of the joints. Due to the small link masses and the high mechanical joint stiffness, vibration damping is not an issue here. Therefore, the approximation $\mathbf{q} = \boldsymbol{\theta} = \bar{\mathbf{q}}$ can be made. While joint and Cartesian impedance control are used for power grasp and independent finger tip motion respectively, the most interesting case from a control point of view is the fine manipulation of a grasped object since all degrees of freedom of the hand can contribute to its motion. In this case the combined system containing arm, hand, and object represents a parallel robot (Fig. 4). The task coordinates consist of two contributions. On the one hand the Cartesian coordinates of the grasped object, on the other hand the coordinates that are related to internal forces.

In [7] we introduced a passivity-based object-level controller for a multifingered hand based on a virtual object similar to [8]. In contrast to the IPC [8] the object frame is defined uniquely by the $i = 1 \dots N$ Cartesian fingertip positions $\mathbf{p}_i(\bar{q})$ by an appropriate kinematic relationship. The definition is such that it enables the spanning of the null-space of the grasp matrix by internal forces generated by virtual

elastic elements connecting the virtual object frame with the finger tips (Fig. 4).

The definition of a potential function $V(\bar{q})$ to derive an object level controller is then described by the superposition of two potentials: the potential of a spatial spring $V_s(\mathbf{H}_{ho}(\bar{q}), \mathbf{H}_{ho,d}, \mathcal{K}_{ho})$ between the virtual object frame $\mathbf{H}_{ho}(\bar{q})$ and a virtual equilibrium frame $\mathbf{H}_{ho,d}$ and a potential $V_{hc}(\bar{q}, \mathcal{K}_{hc})$ describing the i^{th} spring connecting the virtual object with the i^{th} frame of the fingertips $\mathbf{H}_{f,i}(\bar{q})$ for $i = 1 \dots N$ that are used to generate internal forces, i. e.

$$V(\bar{q}) = V_s(\mathbf{H}_{ho}(\bar{q}), \mathbf{H}_{eq}, \mathcal{K}_{ho}) + V_{hc}(\bar{q}, \mathcal{K}_{hc}). \quad (2)$$

The expressions \mathcal{K}_{ho} , \mathcal{K}_{hc} contain the stiffness matrix of the spatial spring and the coupling spring parameters, respectively. The potential for the coupling springs is different from the potentials for spatial springs and is chosen to be spherical for each fingertip i [7]:

$$V_{hc}(\bar{q}, \mathcal{K}_{hc}) = \frac{1}{2} \sum_{i=1}^N K_{hc,i} [\|\Delta \mathbf{p}_i(\bar{q})\| - l_{i,d}]^2, \quad (3)$$

with $\Delta \mathbf{p}_i(\bar{q}) = \mathbf{p}_i(\bar{q}) - \mathbf{p}_{ho}(\bar{q})$ being the distance from the position of the fingertip frame i to the virtual object frame position \mathbf{p}_{ho} , and $K_{hc,i} > 0$ the corresponding coupling stiffness.

B. Employing Impedance Control for Two-Handed Manipulation

A natural extension of the impedance control approaches for the arms and hands allows to formulate intuitive compliance behaviors also for more complex anthropomorphic manipulators like the humanoid manipulator "Justin" (Fig. I-3). This system was built at DLR as a testbed for studying two-handed manipulation tasks. It consists of two four-fingered artificial hands, two lightweight arms, and a sensor head mounted on a movable torso including the neck. Overall, "Justin" has 43 degrees of freedom.

Let us first consider the problem of controlling two arms. The end-effector frames of the right and left arm will be denoted as $\mathbf{H}_r(\bar{q})$ and $\mathbf{H}_l(\bar{q})$, respectively. Similar to multifingered hands, the compliance control of two arms has to handle the interaction forces between the two arms as well as the forces which the two arms exert cooperatively on the environment. The implementation, however, is even simpler in this case and can be done by combining two spatial springs. One spatial spring defines the relative compliance between the arms and can be described in a straight-forward way by the potential function $V_s(\mathbf{H}_r(\bar{q}), \mathbf{H}_l(\bar{q}), \mathcal{K}_c)$. For implementing the cooperative action of the two arms it is useful to rely on a virtual object frame $\mathbf{H}_o(\mathbf{H}_r(\bar{q}), \mathbf{H}_l(\bar{q}))$ depending on the two end effector frames of the right and left arm. This object frame describes a relevant pose in between the arms (usually just the mean between the pose of the right and left arm) and thus represents the pose of a grasped object. This virtual object is then connected via a spatial spring \mathcal{K}_o to a virtual equilibrium pose $\mathbf{H}_{o,d}$. In combination with the coupling stiffness, one thus can intuitively define

an impedance behavior which is useful for grasping large objects with two arms. The resulting potential function is given by

$$V_P(\bar{q}) = V_s(\mathbf{H}_o(\mathbf{H}_r(\bar{q}), \mathbf{H}_l(\bar{q})), \mathbf{H}_{o,d}, \mathcal{K}_o) + V_s(\mathbf{H}_r(\bar{q}), \mathbf{H}_l(\bar{q}), \mathcal{K}_c). \quad (4)$$

In case of a two-handed system such a compliance behavior can easily be combined with the object level compliance potentials designed for artificial hands. Therefore, the virtual visco-elastic springs are attached now to the virtual object frames $\mathbf{H}_{r,o}(\bar{q})$ and $\mathbf{H}_{l,o}(\bar{q})$ of the hands instead of attaching them directly to the end-effectors of the arms (Fig. 5). In combination with the interconnection potentials $V_{hcr}(\bar{q}, \mathcal{K}_{hcr})$ and $V_{hcl}(\bar{q}, \mathcal{K}_{hcl})$ for the right and left hand the complete potential function is now given by

$$V_P(\bar{q}) = V_s(\mathbf{H}_o(\mathbf{H}_{r,o}(\bar{q}), \mathbf{H}_{l,o}(\bar{q})), \mathbf{H}_{o,d}, \mathcal{K}_o) + V_s(\mathbf{H}_{r,o}(\bar{q}), \mathbf{H}_{l,o}(\bar{q}), \mathcal{K}_c) + V_{hcr}(\bar{q}, \mathcal{K}_{hcr}) + V_{hcl}(\bar{q}, \mathcal{K}_{hcl}). \quad (5)$$

Notice that all spatial springs generate joint torques for the arms, hands, as well as for the torso by computing the total derivative of the potential function with respect to the generalized coordinates of the complete mechanism (c.f. (1)). The presented control approach results in a passive closed loop system by design and it is therefore related to other intuitive passivity based control approaches like the IPC [8]. Moreover, the chosen set of virtual spatial springs allows for a conceptually simple physical interpretation and consequently for an intuitive parametrization in any higher-level planning stage.

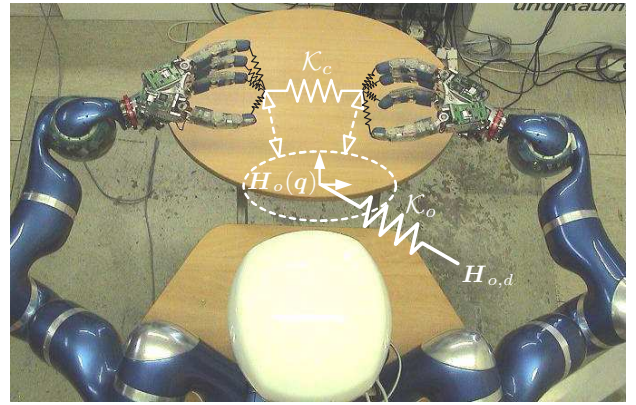


Fig. 5. Two-hand impedance behavior by combining the object level impedances of the hands and the arms.

V. ADJUSTING THE MECHANICAL COMPLIANCE: MOTIVATION OF THE VARIABLE STIFFNESS ACTUATOR DESIGN

A. From Actively Controlled to Passive Compliance

The paradigm of torque controlled light-weight robots was presented in some detail up to now. Various robot examples and the underlying control concepts were introduced. Based

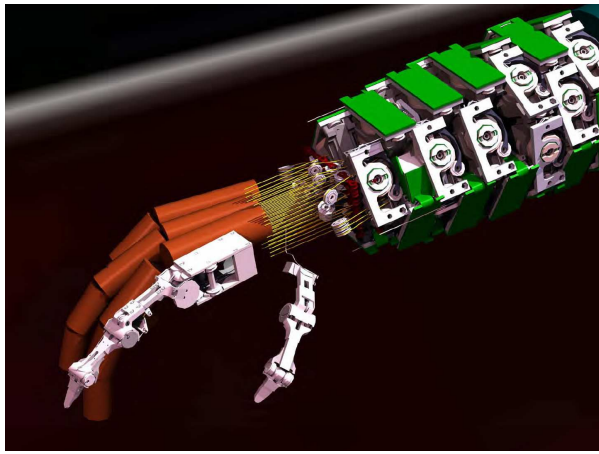


Fig. 6. The integrated DLR Hand-Arm System.

on the experience gained with this successful approach, we were trying to identify also its limitations and recognize new directions of research for further increasing the performance and safety of robots.

The limitations on the achievable compliance⁴ by active control becomes especially an issue when considering the protection of the robot joint from external overload [9]–[11]. This threat can be diminished by deliberately introducing mechanical compliance into the joint. Furthermore, future robotic systems are supposed to execute tasks with similar speed and dexterity to humans. Extreme examples show that humans are capable of generating enormous joint speeds such as shoulder rotation of $6.900 - 9800$ °/s during a baseball pitch of a professional player [12]. This speed range is currently not realizable by robots if the torque range and the weight of the joint should be also compatible with human values. Therefore, new actuation concepts are sought for, in order to approach such requirements. The concept of variable stiffness actuation (VSA)⁵ seems to be a promising solution in this context and its design and control was addressed in numerous publications [9], [13]–[16].

The elastic element serves as an energy storage mechanism, possibly decreasing the energy consumption of the entire system during task execution⁶. Furthermore, the stored energy can be used to considerably increase the link speed as exemplified in Sec. VI-D.1. In contrast to the active compliance case, the robot remains compliant even in case of deactivation or malfunction of the joint, thus potentially increasing the safety of humans interacting with the robot and protecting the robot joint from external impacts.

Our goal is, based on our experience with torque controlled light-weight robots, to built up a fully integrated VSA hand-arm system (Fig. 6) for close, safe and performant interaction

⁴This is due to limited sensor precision, model accuracy, and sampling time as well as due to actuator saturation.

⁵Or its generalization of variable impedance actuation (VIA).

⁶E.g. when playing drums or during running.

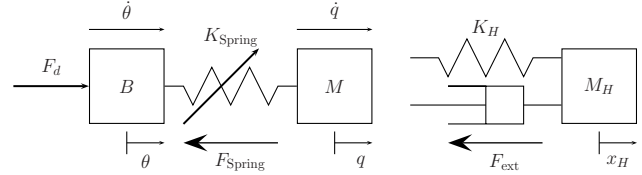


Fig. 7. 1-DOF model of the impact between a variable stiffness robot and a human. The robot is modelled as a mass-spring-mass system, representing the motor mass, joint stiffness and link mass. The human model is a Hunt-Crossley model harmonized with experimental crash test dummy data [11]. B , M were selected to be the reflected inertias in case of a typical stretched out collision configuration with the DLR-LWRIII and K_{Spring} varied according to Fig. 8.

with humans while fulfilling the above requirements as close as possible.

Naturally, such a fundamental paradigm shift comes at a certain cost. The increased number of actuators and the small intrinsic damping⁷ are certainly some of the major challenges in controlling a variable compliance joint. The expected reduction in absolute position accuracy due to the elasticity needs to be compensated by external sensing as e.g. vision. Furthermore, a lower mechanical bandwidth will be the consequence due to the generally lower joint stiffness. Regarding the realizable compliance, the first prototypes are expected to implement a diagonal joint stiffness matrix only. This is posing some limitations on the structure of the achievable Cartesian compliance [17]. However, if necessary, the couplings can still be obtained by active control, as described Sec. III, IV.

In order to exemplify some possible advantages of the VSA design, a preliminary discussion of the influence of joint compliance on human and robot safety is presented, before introducing the hardware design in Sec. VI.

B. Protecting the Robot Joint and the Human by Variable Joint Stiffness

Rigid impacts at high speeds pose an enormous threat to the robot joint [11]. The exceedance of the maximum nominal joint torques are already shown at less than half of the maximum speed of the DLR-LWRIII. This problem necessitates fast collision detection and reaction schemes to prevent damage to the manipulator⁸. In contrast, the VIA actuators limit in an intrinsic way the impact joint torques by elastically decoupling the link from gearbox and motor for the duration of the impact. In order to visualize this effect, a one-dimensional translational example (Fig. 7) was simulated. In Fig. 8 the joint force F_{Spring} during an impact with a human head at 2m/s for a VS-Joint is depicted. One can see that it decreases dramatically for a joint stiffness reduced by one or two orders of magnitude compared to the DLR-LWRIII, thus substantially reducing the load of

⁷Introducing mechanical damping into the system would increase the open loop performance at the cost of higher complexity, weight and energy losses.

⁸Preliminary results indicate this is only possible up to a certain impact velocity which is far below the maximum velocity of the manipulator. Especially the joint-torque sensor and the gears can be severely damaged.

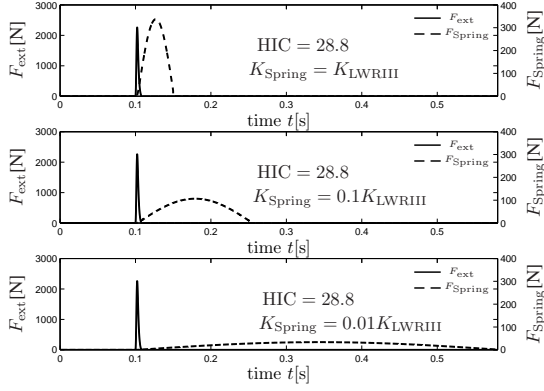


Fig. 8. Effect of joint stiffness reduction on impact force, HIC and spring force during an impact with the human head at 2m/s impact velocity. The spring force decreases in magnitude and increases in duration when lowering the spring stiffness. The joint stiffness K_{Spring} was chosen to be K_{LWRIII} , $0.1K_{\text{LWRIII}}$ and $0.01K_{\text{LWRIII}}$, i.e. 100%, 10%, and 1% of the reflected DLR-LWRIII joint stiffness.

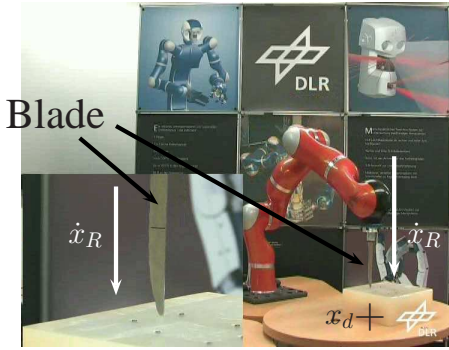


Fig. 9. The DLR-LWRIII equipped with a knife moves along a desired trajectory. The penetrated material is a silicone block. This experiment shows the benefit of intrinsic or controlled joint elasticity during impacts with sharp tools. The goal position x_d was $\approx 7\text{cm}$ inside the silicone block.

the joint. First experimental results confirming the above statements are shown in Sec. VI-D.3.

The possible injury of the human during such rigid impacts is discussed in detail in [11], [18]. It is shown there that the **impact** forces (which are related to the kinetic energy) and thus the potential injury of a human do not depend on the joint stiffness already for link inertias and joint stiffness similar to the ones of the DLR-LWRIII. In Fig. 8 the Head injury Criterion (HIC) and the impact forces F_{ext} are depicted, showing that even with reduced joint stiffness they basically stay the same. This can be explained by the fact that rigid impacts are practically over before the joint force starts rising. In other words it is only the link inertia involved in such hard and rigid impacts.

A case for which compliance of the robot does reduce the injury risk for humans is given by impacts with sharp tools at moderate velocity. This is exemplified by the experiment from Fig 9, in which the DLR-LWR holding a knife moves along a desired trajectory in position or joint impedance controlled mode, penetrating a silicone block. It shows in Fig. 10 that with very low joint stiffness the force and penetration depth increase much slower. For this particular trajectory one

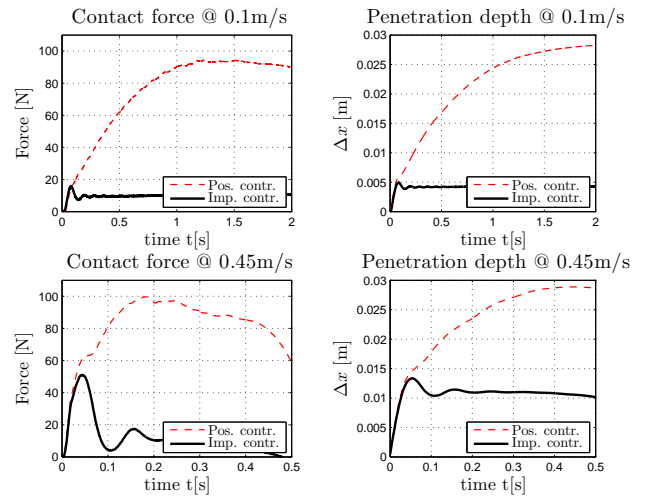


Fig. 10. Contact force and penetration depth for two different Cartesian velocities of 0.1m/s and 0.45m/s. Clearly, the benefit of the reduction of joint stiffness is apparent. The force level can be decreased even below levels which would potentially harm a human, whereas in position control the force significantly exceeds this threshold. The goal position x_d was $\approx 7\text{cm}$ inside the silicone block.

presumably could prevent damaging the human skin⁹. Apart from these benefits, the problem of impacting in a pretensioned state or at very high joint velocities caused by striking out is of major focus for future research. This problem is especially important in the context discussed in Sec. VI-D.1 which shows a vast performance increase concerning link velocity by using the stored potential energy of the joint spring to further accelerate the link inertia. While these two examples are intended to illustrate the benefit of VSA design from the robot safety and performance point of view, the next section will introduce the DLR-VSA design and present some experimental evidence of the performance increase and robot protection. Increasing human safety by VIA design is also a major issue which will constitute the topic of a separate publication.

VI. NEW HARDWARE DESIGN CONCEPTS

The simplest intrinsically compliant joint realization has a fixed spring behavior, usually with a constant or progressive stiffness characteristic. This results in a significant loss of link motion bandwidth. To reduce this effect the stiffness of the joint has to be adaptable to the desired task, requiring a second actuator. Several design approaches realizing robotic joints with variable mechanical stiffness are described in the literature [9], [13]–[16].

The biologically motivated concept of antagonistic actuation can be found already in some robotic systems [20], [14], [21]. In these realizations two opposing actuators of similar size, each in combination with a series elastic element drive

⁹Already contact forces of $< 80\text{N}$ are enough to penetrate the human skin and cause further injury with a knife in case of stabbing [18]. However, with appropriate collision detection strategies, we confirmed in swine experiments that the DLR-LWR can avoid injuries with such sharp tools as knives up to certain velocity [19]. The additional compliance of the actuator will increase the time available to react thus enabling higher maximal velocities.

were used. By running together in the same direction the position is altered and by moving in opposing direction the link stiffness is adjusted (Fig. 12a). Furthermore, unless non-backdrivable gears are used, a high stiffness setting demands a constant torque of both actuators in opposing directions. This has some drawbacks in energy consumption. The approach in [22] aims at a reduction of these effects by motor cross-coupling. As an advantage, the antagonistic principle provides in tendon driven joints an intrinsic robustness to kinematic errors. Furthermore, it is capable of completely distributing the power of both motors to stiffness changes or to the joint motion. The antagonistic principle is applied to the new tendon controlled DLR hand.

Current work at DLR regarding robot arm joints is focused on a second option, in which one motor changes the link position and the other one the link stiffness almost independently [23]. This system leads to reduced dynamic losses and allows for stiffness adjustment independent from the link speed.

In our approach the positioning motor is connected to the link via a harmonic drive gear. Mechanical compliance is introduced by a mechanism, which forms a flexible rotational support between the harmonic drive gear and the joint base (Fig. 11). In case of a compliant deflection of the joint, the whole harmonic drive gear rotates relatively to the base, but the positioning motor is not moved. So the link side inertia is altered only by the circular spline and some parts of the variable stiffness device. In contrast to that, the spring mechanism adds no inertia to the drive train between the positioning motor and the link. The link position is changed without moving the elasticity mechanism.

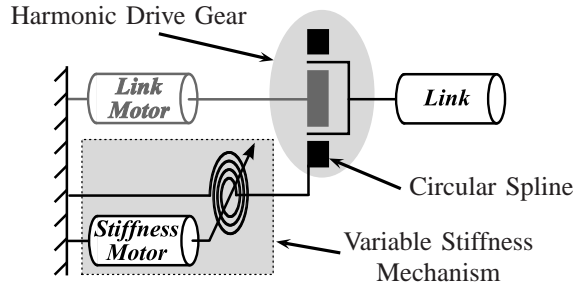


Fig. 11. Principle of variable stiffness joint mechanics. The circular spline of the harmonic drive gear is supported by the new mechanism.

Two different mechanical compliant joint principles (patents pending) are derived from the previous considerations. A short overview of the principles is given in the following.

A. Quasi Antagonistic Joint Mechanism

The elastic mechanism of the Quasi Antagonistic Joint is derived from the antagonistic principle: Two progressive elastic elements oppose each other with a variable offset supporting the link with variable range of elastic motion (Fig. 12).

The previously mentioned harmonic drive gear for link positioning is held in a bearing and has a cam bar attached to its normally fixed part (Fig. 13). Two pairs of rocker arms act on different faces of this cam bar. External loads result in rotational displacement of the whole gear and force the rocker arms to spread against a linear spring causing progressive restoring torque. The agonist rocker arms are fixed to the housing to save energy, while the antagonist part is positioned at a rotational offset by a stiffness actuator, which can change the stiffness very quickly and independent from the link speed (Fig. 12.b).

The shape of the cam faces can be designed to provide the desired restoring torque characteristic. Superposition of agonist and antagonist forces with different offsets results in variable stiffness. In the nominal range it has (close to) linear behavior and gets progressive towards the ends of the range for joint protection.

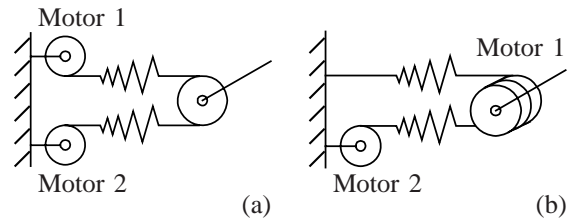


Fig. 12. Variable Stiffness Actuator with nonlinear progressive springs in antagonistic (a) and quasi antagonistic (b) realization. In the later case, Motor 1 moves the joint while Motor 2 is adjusting the stiffness.

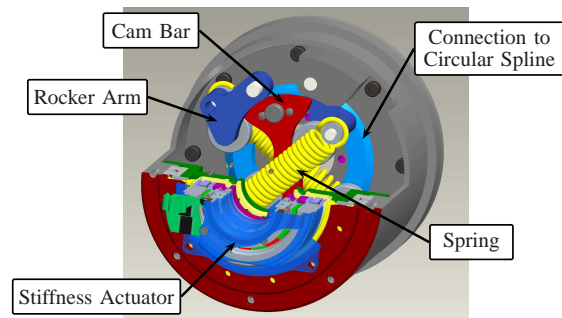


Fig. 13. Cross section of the Quasi Antagonistic Joint design.

B. Variable Stiffness Joint Design

The concept of the Variable Stiffness Joint (VS-Joint) as presented in [24] contains two motors of different size. The high power motor changes the link position. The joint stiffness is adjusted by a much smaller and lighter motor, that changes the characteristic of the supporting mechanism (Fig. 14). An unwinded schematic of the principle is shown in Fig. 15. A compliant link deflection results in a displacement of the cam disk and is counterbalanced by the roller pressed on it in axial direction by a spring. This generates a centering force resulting in the output torque of the link. To change the stiffness preset, the smaller motor moves the spring base axially relative to the cam disk and thus varies the spring force. The joint prototype can be equipped with different cam disks. This permits an easy adaption of the

passive joint behavior to the desired application by designing the torque/deflection characteristic of the joint.

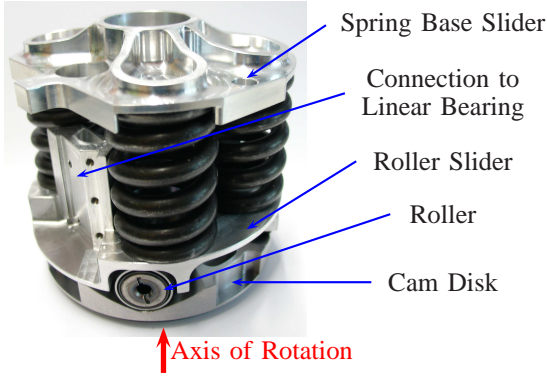


Fig. 14. VS-Joint mechanism. The link axis is in the vertical direction. The cam disk rotates on a compliant link deflection.

C. Control of Variable Impedance Actuators

Regarding the control of VIA, the literature mostly deals with the problem of adjusting stiffness and position of the actuator in a decoupled manner, by controlling the position or the torque of the two motors of the joint [13], [15], [16]. Moreover, in case of VSA structures with many dof and cable actuation, the decoupling of the tendon control is treated [25], [26].

Our approach to the control of the VSA arms is to extend the passivity based control framework developed for the torque controlled light-weight robots to the VSA case. Some particular aspects compared to the controllers from Sec. III, IV are summarized below:

- Due to the high compliance of the joint, a separate torque sensor is not required any more, the torque can be well estimated based on the motor and link position [24].
- An active compliance control will be used only for stiffness components which cannot be realized by the mechanical springs. Examples are zero stiffness or the joint coupling stiffness needed by arbitrary Cartesian stiffness matrices [17].
- The joints have very low intrinsic damping. While this is useful for cyclic movements, involving energy storage (e.g. for running), the damping of the arm for fast, fine positioning tasks has to be realized by control. This is

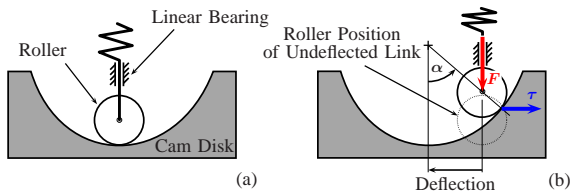


Fig. 15. Unwinded schematic of the VS-Joint principle in centered (a) and deflected (b) position. A deflection of the link results in a horizontal movement of the cam disk and a vertical displacement of the roller. The spring force generates a centering torque on the cam disk.

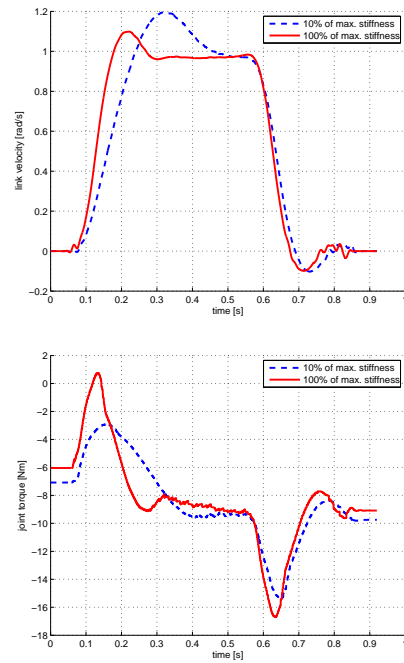


Fig. 16. Motion on a trajectory with rectangular velocity profile for small and maximal stiffness. A critically damped velocity step response can be achieved independent from the stiffness and inertia value (upper). The effect of vibration damping is clearly observed in the torque signal (lower).

a challenging task, regarding the strong variation of the inertia and the stiffness. Fig. 16 shows the performance of the positioning for a very low as well as for a very high stiffness preset of the VS-Joint.

- Absolute accuracy of fine manipulation has to be realized using additional external sensing at the tip.
- The antagonistically tendon-driven joints of the hand (Fig. 6) require the extension to handle nonlinear coupled joints based on the tendon coupling matrix.
- The pulling constraint of the tendons has to be fulfilled strictly. Decoupling algorithms will be used to ensure the realization of the passive joint stiffness while the active joint stiffness can be varied over a large domain. Furthermore, a quasi-static effective joint stiffness can be given as a setpoint.

D. Performance Validation

Along with the activity regarding the control of the joint, first experiments for validating the increase in performance were done.

1) *Throwing*: The application of throwing a ball is a good example to show the performance enhancement gained by the VS-Joint in terms of maximal velocity. For throwing a ball as far as possible, it has to be accelerated to the maximum achievable velocity and released at an angle of 45° . The link velocity of a stiff link corresponds to the velocity of the driving motor. In a flexible joint the potential energy stored in the system can be used to accelerate the link relatively to the driving motor. Additional energy can be inserted by the stiffness adjuster of the variable stiffness joint to gain an

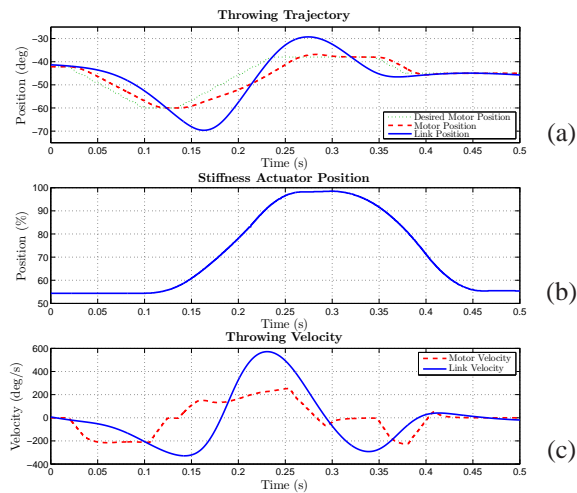


Fig. 17. Throwing trajectory (a), stiffness motor position (b) and joint velocities (c).

even faster motion.

A lacrosse stick head was mounted on the top of the link lever for the throwing tests. The ball is a 64 g rubber ball for school lacrosse. The distance between the link axis and the center of the ball when the ball leaves the lever is approximately 0.78 m.

A simple strike out trajectory is used to gain high link velocity (Fig. 17). It uses the resonance effect of the mass-spring system to maximize joint velocity. With the measured maximum link velocity of 572° s^{-1} , the throwing distance was approximately 6 m, corresponding well to the calculated distance of 6.18 m. The theoretical throwing distance with an inelastic link of the same setup with the same maximum motor velocity of 216° s^{-1} is 0.88 m, also confirmed experimentally. A speed gain of 265% for the link velocity between rigid and compliant joint was achieved in the test.

Compared to a human, the throwing range of the VS-Joint seems small, but one has to keep in mind that this was done by a single joint whereas a human uses several degrees of freedom including the hip joints. A series arrangement of joints in a robot arm enlarges the achievable distance.

2) *Stiffness Adjustment*: While a similar increase of velocity could also be realized by a series elastic actuator without adjustable stiffness, Fig. 16 shows the advantage of the VSA design. Fast positioning can be achieved by increasing the stiffness. On the other hand, lowering the stiffness can be used in certain situations for protecting the robot from external loads, as described in Sec. V-B and validated by the following experiment¹⁰.

3) *Experimental Validation of Joint Overload Protection*: In order to validate the results from Sec. V-B, the impact of the joint at a predefined velocity with a test object was evaluated. Two stiffness setups are realized via the passively compliant VS-Joint. The most compliant as well

¹⁰A paper with detailed discussion of the load reduction of the joint is currently in preparation.

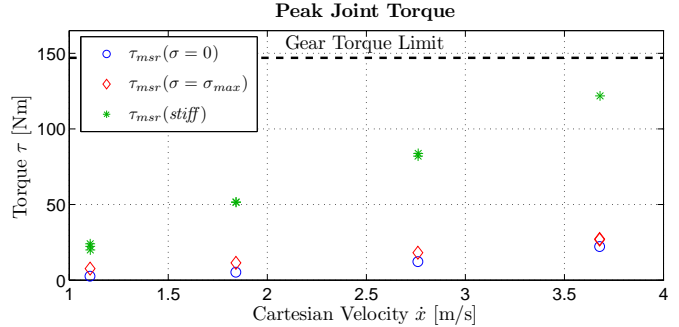


Fig. 18. Peak joint torque during impacts with the VS-Joint. The impact velocity ranges up to the maximum velocity of the KR500/Robocoaster on which the joint was mounted for the experiment.

as the stiffest configuration were chosen. In a third setup a mechanical shortcut is inserted into the test-bed instead of the VS-Joint mechanism such that a much stiffer joint is obtained¹¹.

Both, increasing impact speed and increasing joint stiffness result in higher peak joint torques as visualized in Fig. 18. The maximum peak torque limit of the joint gear is almost reached with the stiff joint at an impact velocity of ≈ 3.7 m/s, whereas the compliant VS-Joint is still far in the safe torque region.

VII. CONCLUSIONS

In this paper we gave an overview on the DLR activities related to two approaches for the realization of soft robotics: actively torque controlled light-weight robots and variable stiffness actuation. Based on our experience with torque controlled robots, we presented an analysis on expected advantages and also disadvantages of VSA actuators. Furthermore, two VSA joint designs motivated by this analysis were presented.

While torque-controlled robots currently represent currently a technology that is mature enough to go to market, we believe impressive research progress can be expected in the area of VSA actuated robots within the next decade.

REFERENCES

- [1] A. Albu-Schäffer, C. Ott, and G. Hirzinger, "A unified passivity based control framework for position, torque and impedance control of flexible joint robots," *The Int. J. of Robotics Research*, vol. 26, no. 1, pp. 23–39, 2007.
- [2] C. Ott, A. Albu-Schäffer, A. Kugi, and G. Hirzinger, "On the passivity based impedance control of flexible joint robots," *IEEE Transactions on Robotics and Automation*, vol. 24, no. 2, pp. 416 – 429, 2008.
- [3] A. Albu-Schäffer, C. Ott, and G. Hirzinger, "A passivity based cartesian impedance controller for flexible joint robots - Part II: Full state feedback, impedance design and experiments," *IEEE Int. Conf. of Robotics and Automation*, pp. 2666–2673, 2004.
- [4] E. Fasse and J. Broenink, "A spatial impedance controller for robotic manipulation," *IEEE Transactions on Robotics and Automation*, vol. 13, no. 4, pp. 546–556, 1997.
- [5] F. Caccavale, C. Natale, B. Siciliano, and L. Villani, "Six-dof impedance control based on angle/axis representations," *IEEE Transactions on Robotics and Automation*, vol. 15, no. 2, pp. 289–299, 1999.

¹¹In the range of the DLR-LWRIII joint elasticity.

- [6] S. Stramigioli and V. Duindam, "Variable spatial springs for robot control applications," in *IEEE/RSJ International Conference on Intelligent Robots and Systems*, 2001, pp. 1906–1911.
- [7] T. Wimböck, Ch. Ott, and G. Hirzinger, "Passivity-based object-level impedance control for a multifingered hand," in *IEEE/RSJ International Conference on Intelligent Robots and Systems*, 2006, pp. 4621–4627.
- [8] S. Stramigioli, *Modeling and IPC Control of Interactive Mechanical Systems: A Coordinate-free Approach*, ser. Lecture Notes in Control and Information Sciences. Springer-Verlag, 2001, vol. 266.
- [9] T. Morita, H. Iwata, and S. Sugano, "Development of human symbiotic robot: Wendy," *IEEE Int. Conf. of Robotics and Automation*, pp. 3183–3188, 1999.
- [10] S. Haddadin, T. Laue, U. Frese, and G. Hirzinger, "Foul 2050: Thoughts on physical interaction in human-robot soccer," in *IEEE/RSJ International Conference on Intelligent Robots and Systems (IROS2007), San Diego, USA, 2007*, pp. 3243–3250.
- [11] S. Haddadin, A. Albu-Schäffer, and G. Hirzinger, "Safety Evaluation of Physical Human-Robot Interaction via Crash-Testing," *Robotics: Science and Systems Conference (RSS2007), Atlanta, USA*, download: <http://www.roboticsproceedings.org/rss03/p28.html>, 2007.
- [12] I. P. Herman, *Physics of the Human Body*. Springer Verlag, 2007.
- [13] A. Bicchi and G. Tonietti, "Fast and Soft Arm Tactics: Dealing with the Safety-Performance Trade-Off in Robot Arms Design and Control," *IEEE Robotics and Automation Mag.*, vol. 11, pp. 22–33, 2004.
- [14] S. A. Migliore, E. A. Brown, and S. P. DeWeerth, "Biologically Inspired Joint Stiffness Control," in *IEEE Int. Conf. on Robotics and Automation (ICRA2005), Barcelona, Spain, 2005*.
- [15] G. Palli, C. Melchiorri, T. Wimboeck, M. Grebenstein, and G. Hirzinger, "Feedback linearization and simultaneous stiffness-position control of robots with antagonistic actuated joints," in *IEEE Int. Conf. on Robotics and Automation (ICRA2007), Rome, Italy, 2007*, pp. 2928–2933.
- [16] B. Vanderborght, B. Verrelst, R. V. Ham, M. V. Damme, D. Lefeber, B. M. Y. Duran, and P. Beyl, "Exploiting natural dynamics to reduce energy consumption by controlling the compliance of soft actuators," *Int. J. Robotics Research*, vol. 25, no. 4, pp. 343–358, 2006.
- [17] A. Albu-Schäffer, M. Fischer, G. Schreiber, F. Schoeppe, and G. Hirzinger, "Soft robotics: What cartesian stiffness can we obtain with passively compliant, uncoupled joints?" *IEEE Int. Conf. on Intelligent Robotic Systems*, pp. 3295–3301, 2004.
- [18] S. Haddadin, A. Albu-Schäffer, and G. Hirzinger, "Safe Physical Human-Robot Interaction: Measurements, Analysis & New Insights," in *International Symposium on Robotics Research (ISRR2007), Hiroshima, Japan, 2007*.
- [19] S. Haddadin, A. Albu-Schäffer, A. De Luca, and G. Hirzinger, "Evaluation of Collision Detection and Reaction for a Human-Friendly Robot on Biological Tissues," in *IARP International Workshop on Technical challenges and for dependable robots in Human environments (IARP2008), Pasadena, USA, 2008*.
- [20] K. Koganezawa, "Mechanical stiffness control for antagonistically driven joints," in *Proc. of the IEEE/RSJ International Conference on Intelligent Robots and Systems*. IEEE/RSJ, August 2005, pp. 2512–2519.
- [21] C. English and D. Russell, "Implementation of variable joint stiffness through antagonistic actuation using rolamite springs," *Mechanism and Machine Theory*, vol. 34, no. 1, pp. 27–40, 1999.
- [22] G. Tonietti, "Variable Impedance Actuation," Ph.D. dissertation, University of Pisa, 2005.
- [23] T. Morita and S. Sugano, "Development and evaluation of seven-d.o.f. mia arm," in *Proc. 1997 IEEE International Conference on Robotics and Automation*, September 1997, pp. 462–467.
- [24] S. Wolf and G. Hirzinger, "A new variable stiffness design: Matching requirements of the next robot generation," in *IEEE Int. Conf. on Robotics and Automation*. Pasadena, USA: IEEE, 2008, pp. 1741–1746.
- [25] H. Kobayashi and R. Ozawa, "Adaptive neural network control of tendon-driven mechanisms with elastic tendons," *Automatica*, vol. 39, pp. 1509–1519, 2003.
- [26] K. Tahara, Z.-W. Luo, R. Ozawa, J.-H. Bae, and S. Arimoto, "Biomimetic study on pinching motions of a dual-finger model with synergistic actuation of antagonist muscles," in *IEEE International Conference on Robotics and Automation*, 2006, pp. 994–999.